Int J Thermophys (2008) 29:1422–1438
DOI 10.1007/s10765-008-0498-6

In-plane Thermal Diffusivity Measurement of Thin Samples Using a Transient Fin Model and Infrared Thermography

L. Miettinen · P. Kekäläinen · J. Merikoski · M. Myllys · J. Timonen

Received : 13 December 2007 / Accepted: 21 July 2008 / Published online: 12 August 2008

Abstract A method for determining the in-plane thermal diffusivity of planar samples was constructed. The time-dependent temperature field of the sample heated at one edge was measured with an infrared camera. The temperature fields were averaged for different times over a narrow strip around the center line of the sample, and the temperature profiles for varying time were fitted by a solution to a corresponding one-dimensional heat equation. Heat losses by convective and radiative heat transfer were both included in the model. Two fitting parameters, the thermal diffusivity and the effective heat-loss term, were obtained from time-dependent temperature data by optimization. The ratio of these two parameters was also extracted from the steady-state temperature profile. The method was found to give good and consistent results when tested on copper and aluminum samples.

Keywords IR camera · Solid material · Thermal conductivity · Thermal diffusivity · Thermal imaging

1 Introduction

In this article we describe a method for determining the in-plane thermal diffusivity $k/\rho c_p$ in planar geometry. The method is based on measuring the transient temperature field in a sample using an infrared camera and fitting the data by a theoretical solution, $k/\rho c_p$ as one of two fitting parameters. With a known constant density ρ and specific heat capacity c_p, the thermal conductivity k of the sample can also then be determined.

L. Miettinen (✉) · P. Kekäläinen · J. Merikoski · M. Myllys · J. Timonen
Department of Physics, University of Jyväskylä, P. O. Box 35 (YFL),
40014 Jyväskylä, Finland
e-mail: lasse.miettinen@phys.jyu.fi

There already exist many measurement methods for thermal diffusivity (see, e.g., [1]). The flash technique [2,3] is widely used, and it has also been applied to in-plane measurements [4]. Heating of the sample can as well be arranged by a simple heating element, while the temperature field is measured by an infrared camera [5]. Instead of measuring the time evolution of temperature at two points [5], we extend this method and use, e.g., the whole temperature profile in a planar sample. In addition, we increase the accuracy of this method by also reducing the effect of heat losses on the measured thermal diffusion coefficient. We model the convective and radiative heat transfer, and determine the linearized heat-loss coefficient when determining the thermal diffusion coefficient. To this end, a weak flow of air is also included around the sample to stabilize the convective heat transfer.

A motivation for using a simple heating element is that by this method we can easily produce a linear temperature front propagating in the sample. This measuring geometry allows one-dimensional modeling (provided that the relevant Biot number is much less than unity, see below), and different heat-loss mechanisms can more easily be included in the model. When we furthermore calibrate the temperature of each sample as determined by the infrared camera, the true emission coefficient of the sample is automatically taken into account. With this kind of method, we can thus achieve very good accuracy for the measured temperatures, as evidenced by the results reported below. We can therefore extend the method of this work to the case where thermal diffusivity and heat-loss coefficients depend on temperature, and determine as well their temperature dependence.

2 Experimental Setup

The experimental setup is shown schematically in Fig. 1. A sample plate initially at room temperature is pressed suddenly between two copper plates heated by electric resistors. These resistors are covered in Teflon casings so as to minimize heat losses. The two heating resistors are connected in series, and the heating power can be adjusted.

Under the sample there is a 100 mm diameter pipe and a fan which are used to introduce a slow, laminar air flow over the plate in order to keep constant the convective heat transfer from the sample. A part of the pipe is filled with porous material to damp turbulence and to homogenize the air flow. The fan speed can be controlled. The whole experimental setup is located in a room in which all disturbing air flows have been eliminated.

The time-dependent temperature field in the sample is recorded with an infrared camera, and a PC is connected to the camera for image grabbing and further data analysis. There is a chamber around the system for shielding it from anomalous heat radiation from the surroundings. A total of 25 images per second were recorded in the measurements, and the spatial resolution of the measured temperature field was typically about 0.3 mm.

The emittance of the samples was improved by painting them thinly on both sides with black spray paint before measurements. The IR camera was then calibrated for each sample by attaching a thermocouple on the sample surface and measuring the

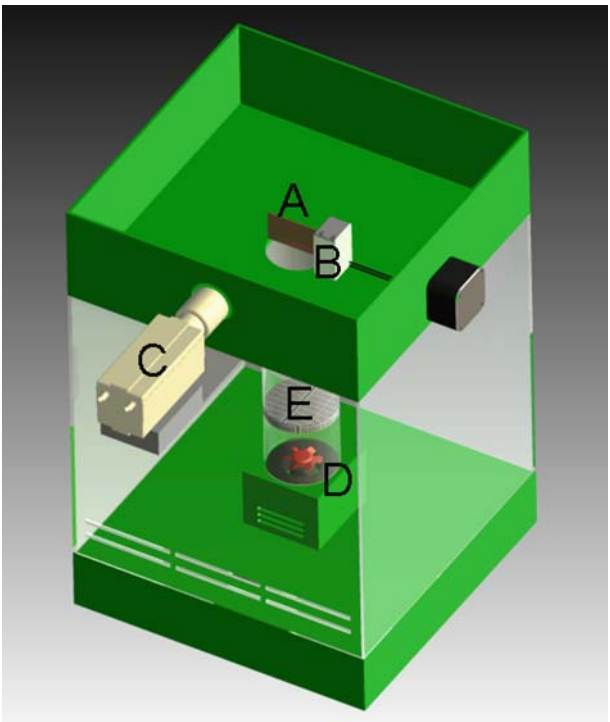

Fig. 1 Schematic diagram of the experimental setup. The upper part of the measuring chamber is not shown. A is the sample, B is the heating unit, C is the IR camera, D is the fan, and E is the flow controller

temperature of that point with the IR camera. The procedure was repeated for several different plate temperatures, and a calibration curve was eventually achieved. Calibration data together with polynomial least-squares fits for copper and an aluminum plate are shown in Fig. 2. A fifth-order polynomial fit was used for the copper sample and a third-order fit for the aluminum. The small differences between the calibration curves may be caused by slightly different emittances, and their temperature dependences, of the two samples. The emittance values were not determined because the calibration curves give accurately the needed temperature data from the IR-camera images.

It is essential that the sample plate can be accurately cropped from the IR-camera image. The temperature field was usually too blurry at the plate edges to distinguish the sample clearly from the background, especially at the cooler edge of the plate. Therefore, the position of each edge of the plate was first marked by holding an electrically heated tungsten wire on the edge for a while. The hot wire stood out from the background in the image, and the center line of the wire determined the position of the edge in the recorded temperature field. This cropping procedure had to be carried out every time a sample was installed in the holder for measurements.

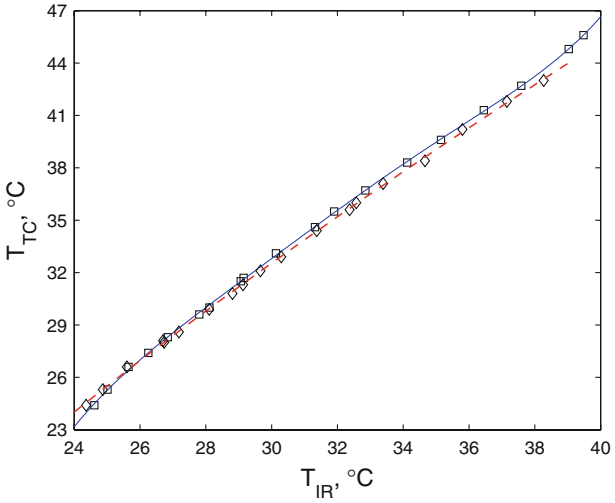

Fig. 2 Calibration curve of the IR camera for a 1.0 mm thick copper plate (squares and the solid line) and for a 1.0 mm thick aluminum plate (diamonds and the dashed line). The "accurate" temperatures T_{TC} were measured by a thermocouple attached to the plate

3 Mathematical Model

Since a whole edge of the planar sample is heated and the boundary conditions are similar at the two adjacent plate edges, the system is symmetric in the direction away from the heater. Provided that the sample thickness is much less than the ratio of the heat diffusion coefficient α to the effective heat-loss rate coefficient η (see below), i.e., that the relevant Biot number is much less than unity, we can also assume that the sample is isothermal in the thickness direction. Now we could solve the remaining two-dimensional heat equation, but if we restrict our consideration to a narrow strip at the center line of the plate, we can use a one-dimensional heat equation to describe the system;

$$\rho c_p \frac{\partial T}{\partial t} = \frac{\partial}{\partial x}\left(k\frac{\partial T}{\partial x}\right) + \dot{q}. \tag{1}$$

Here $T = T(x, t)$ is the temperature of the plate with x the distance from the heated edge of the plate, c_p is the specific heat, ρ is the density, k is the thermal conductivity (more precisely the x component of the thermal-conductivity tensor) of the material of the plate, and $\dot{q}$ is the rate at which energy is generated (lost or gained) per unit volume of the medium. The energy generation term includes convective and radiative heat transfer;

$$\dot{q} = -\frac{2h}{a}(T - T_\infty) - \frac{2\varepsilon\sigma}{a}(T^4 - T_{\mathrm{sur}}^4). \tag{2}$$

Here a is the thickness of the plate, h is the convection heat transfer coefficient, ε is the emissivity, and σ is the Stefan–Boltzmann constant. T_∞ is the air temperature, and

T_{sur} the temperature of the walls of the measuring chamber. In our case, $T_{\text{sur}} = T_\infty$. As temperature differences are quite small, we approximate the radiation term by a first-order term in $T - T_\infty$, and find

$$\frac{\partial \Theta}{\partial t} = \frac{\partial}{\partial x}\left(\alpha \frac{\partial \Theta}{\partial x}\right) - \frac{2\eta}{a}\Theta, \tag{3}$$

where $\Theta := T - T_\infty$, $\alpha := k/\rho c_p$ is the heat diffusion coefficient, and $\eta := (h + 4\varepsilon\sigma T_\infty^3)/\rho c_p$ is an effective heat-loss rate coefficient.

One edge of the plate is heated, and the time-dependence of its temperature $\Theta(0, t)$ is measured. At the opposite edge we have convective and radiative heat transfer. So, in Eq. 3, we impose the initial and boundary conditions:

$$\begin{cases} \Theta(x, 0) = f(x), \\ \Theta(0, t) = \Theta_0(t), \\ \alpha \dfrac{\partial \Theta(L, t)}{\partial x} + \eta \Theta(L, t) = 0, \end{cases} \tag{4}$$

where L is the length of the plate. The initial temperature distribution $f(x)$ and the temperature $\Theta_0(t)$ are obtained from measurements.

If α and η are constants, the boundary value problem can be solved as described in Appendix A. The unknown coefficients α and η can then be determined by minimizing the integral,

$$\int_{x_1}^{x_2} \left(\int_{t_1}^{t_2} \left(\Theta_{(\alpha,\eta)}(x, t) - \bar{\Theta}(x, t)\right)^2 \mathrm{d}t \right) \mathrm{d}x \tag{5}$$

with respect to α and η. Here $\Theta_{(\alpha,\eta)}$ is the solution of the boundary value problem, Eq. 3 with Eq. 4, and $\bar{\Theta}$ is the observed temperature. By this choice of the integral form, we take full advantage of the position and time information of the measured temperature data.

For a stationary temperature distribution, we can reduce this two-dimensional optimization problem into a one-dimensional problem in the following way. A stationary temperature distribution satisfies the differential equation,

$$\alpha \frac{d^2\Theta}{dx^2} - \frac{2\eta}{a}\Theta = 0 \tag{6}$$

with the boundary conditions,

$$\begin{cases} \Theta(0) = \Theta_0 \\ \alpha \dfrac{d\Theta}{dx}(L) + \eta \Theta(L) = 0. \end{cases} \tag{7}$$

The solution of this problem is

$$\Theta(x) = \Theta_0 \left(\frac{\cosh \beta(L-x) + (\eta/\beta\alpha) \sinh \beta(L-x)}{\cosh \beta L + (\eta/\beta\alpha) \sinh \beta L} \right) \tag{8}$$

where $\beta^2 = 2\eta/a\alpha$. From the data we get Θ_0 and the ratio η/α is determined by minimizing the integral,

$$\int_{x_1}^{x_2} \left(\Theta(x) - \overline{\Theta}(x)\right)^2 \mathrm{d}x, \tag{9}$$

where $\overline{\Theta}(x)$ is the measured stationary temperature profile. Since we now know the ratio of the two fitting parameters of the time-dependent case, Eq. 5, it is better to use η/α and α as the actual fitting parameters rather than η and α. The other reason for this choice is that the eigenvalues β_n in the solution of the time-dependent case (see Eq. A9 in Appendix A) are functions of η/α, and it is possible to save computation time by selecting this variable as a fitting parameter. The data are thus analyzed in the following way. Optimization with respect to the η/α parameter is done for the steady-state temperature profile (Eq. 9). Thereafter a two-dimensional optimization of the time-dependent temperature profiles is performed (Eq. 5) such that minimization is searched around the η/α value obtained for the steady-state profile.

4 Results

Homogeneous samples with known thermal-conductivity properties were used to validate the method. The sample plates were approximately 50 mm by 100 mm in size and 1.0 mm thick. There were two sample materials: high-purity copper and industrial aluminum. For the copper sample the manufacturer provided the material specifications but for the other sample tabulated properties for pure aluminum were used. The properties are shown for both materials in Table 1. For more thermal-conductivity data as a function of temperature, see Refs. [7] and [8]. It was known that the aluminum sample was not pure, but its properties were assumed not to differ too much from the tabulated values of pure material. In the mathematical model above, it was assumed that the thermal conductivity and the specific heat capacity do not depend on temperature. These assumptions are well satisfied for the two materials when the temperature differences within the samples are relatively small.

Table 1 Density, specific heat capacity, thermal conductivity, and thermal diffusivity of the samples. Values for copper were given by the manufacturer but the other values were taken from Ref. [6] for pure aluminum

Sample	ρ (kg · m^{-3})	c_p (J · kg^{-1} · K^{-1})	k (W · m^{-1} · K^{-1})	α (10^{-3} m^2 · s^{-1})
Cu	8,940	385	399	0.1159
Al	2,702	903	237	0.0971

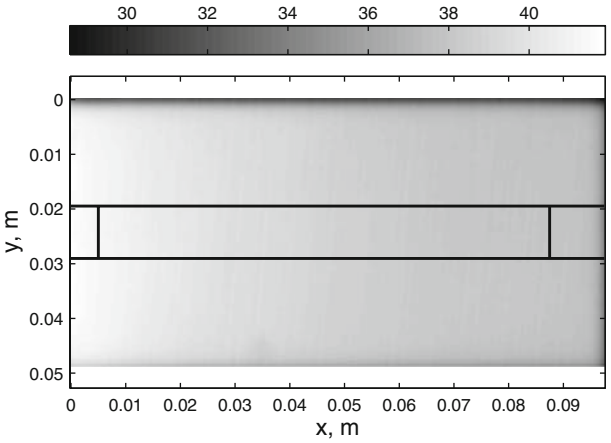

Fig. 3 Steady-state temperature field (averaged over 30 s) of a copper plate recorded by an IR camera. The gray scale bar corresponds to temperature values in °C. The temperature values were corrected using the calibration curve of Fig. 2. The horizontal lines show the averaging window for which a one-dimensional temperature profile is calculated. The small vertical lines are the boundaries for fitting the temperature profile by Eq. 8 (see Fig. 4)

A sample plate was initially at room temperature and was then suddenly pressed between two heating plates. The time-dependent temperature field in the sample was recorded from starting the heating for about two minutes, when the temperature profile was already approaching the stationary one. The sample was left heated in the holder for about an hour, after which the steady-state temperature profile was recorded. Figure 3 shows a steady-state temperature field in a 1 mm thick copper plate.

One-dimensional temperature profiles $T(x, t)$ (see Figs. 4 and 5) were obtained from the temperature fields by taking an average in the y direction over the central fifth of the sample (see Fig. 3). The temperature seems to drop rapidly at the cooler edge of the plate as the IR camera receives radiation there also from confining walls at room temperature. When fitting experimental data by Eqs. 3 and 4, or by Eq. 8 in the steady state, about 10 mm stretches at the edges in the x direction were left out of the fit. The averaging window and the fitting boundaries are marked in Fig. 3. Noise in the temperature profiles were reduced by taking a moving average over an about 2-mm wide window.

A typical time evolution of the average temperature profile in a copper plate is shown in Fig. 5. The measured data were averaged over every five frames, i.e., over 0.2 s, to smooth the time evolution. The initial and boundary conditions, Eq. 4, for the solution of the heat equation, Eq. 3, can be determined from the measured data. The boundary condition $\Theta(0, t)$ was chosen as the temperature difference $T(x) - T_\infty$ at about 10 mm away from the heating edge. The position of the selected boundary is at $x = 0$ in Fig. 5, i.e., the x axis is shifted by 10 mm to the right compared to Fig. 4. A fourth-order polynomial was fitted to the initial spatial temperature profile (the lowest profile in Fig. 5) and to the time dependence of the boundary temperature. These fits were used as $\Theta(x, 0)$ and $\Theta(0, t)$, respectively, when determining the corresponding solution for the heat equation.

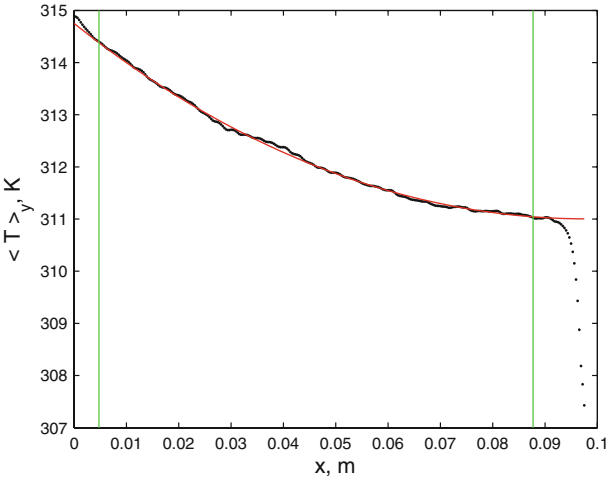

Fig. 4 Steady-state temperature profile (dots) of a copper plate together with a theoretical fit (continuous line). The fitting window is between the two vertical lines. The best fit was found for the fitting-parameter value $\eta/\alpha = 0.0276\,\mathrm{m}^{-1}$. The air temperature was $T_\infty = 297.8\,\mathrm{K}$ in this measurement

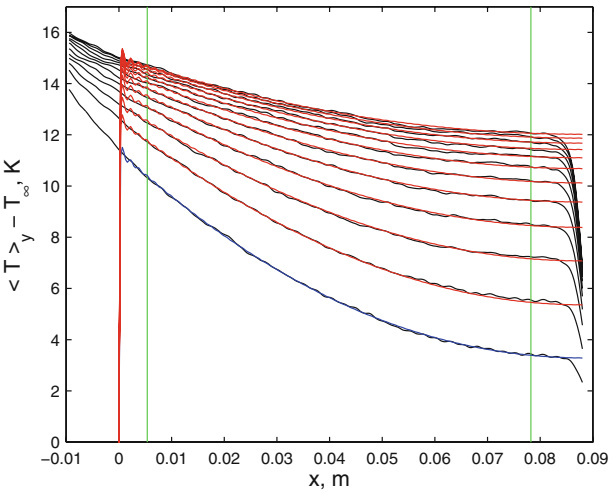

Fig. 5 Transient average temperature profile of a copper plate at 10 s intervals. A fourth-order polynomial is fitted to the first (lowest) profile and is taken as the initial condition for the theoretical solution of the heat equation. The (time-dependent) boundary condition is taken at $x = 0$, and the two vertical lines show the integration region for optimization. The smooth lines for $x > 0$, $t > 0$ represent the theoretical solution with optimized values for η/α and α

Solutions for the heat equation (Eq. 3) were determined for several values of the fitting parameters η/α and α. In this way it was possible to scan the two-dimensional (η, α) parameter space and check if the cost-function minimum is really reached with the same η/α value that gave the best fit for the steady-state temperature profile.

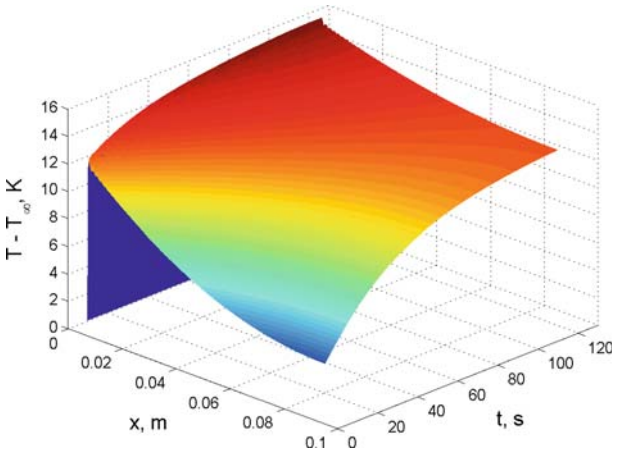

Fig. 6 Solution of the heat equation calculated by using the best-fit parameters for η/α and α. The boundary and initial conditions for the solution were taken from the experimental data for a copper sample (see Fig. 5)

A solution for the copper measurement of Fig. 5 is shown in Fig. 6. The temperature profiles were calculated for the same time values as the experimental data were obtained. Parameter values that minimize the cost function (Eq. 5) are assumed to give the best fit to the data. The solution is not continuous at $x = 0$ (see Appendix A), but such boundary effects are left out of the spatial integration region in the cost function (Eq. 5). The integration limits are shown in Fig. 5. The temporal integration was carried out over all available times.

The cost function for a copper sample, normalized by the integration area, is shown in Fig. 7 as a function of α for different η/α ratios. It turned out that in this case the minimum was found for $\eta/\alpha = 0.0274\,\mathrm{m}^{-1}$ and $\alpha = 1.161 \times 10^{-4}\,\mathrm{m}^2 \cdot \mathrm{s}^{-1}$. The η/α value obtained differed from the steady-state value of $0.0276\,\mathrm{m}^{-1}$ by 0.7 %. The bottom of the cost-function surface in the (η, α) space is quite flat, as can be seen from the contours in Fig. 8, and finding the minimum accurately is sensitive to the η/α value.

Figure 9 shows the difference between the measured average temperature in a copper plate and the solution of the heat equation calculated by using the best-fit parameter values $\eta/\alpha = 0.0274\,\mathrm{m}^{-1}$ and $\alpha = 1.161 \times 10^{-4}\,\mathrm{m}^2 \cdot \mathrm{s}^{-1}$. The square of this difference is actually integrated when determining the value of the cost function. The square root of the cost-function minimum gives a measure for the mean deviation between the theoretical solution and experimental data. In the case of Fig. 9, the minimum of the normalized cost function was $I_{\mathrm{norm}} = 0.00239\,\mathrm{K}^2$ (see Fig. 7), which means that the mean deviation of the solution from the measurement data is 0.05 K. This is actually less than the temperature resolution of the IR camera (0.1 K). The narrow ridges that can be seen in Fig. 9 are caused by Fourier components of the theoretical solution that are summed in Eq. A21. The solution was calculated by using the first 1,000 terms in the summation. This phenomenon became visible because the temperature accuracy was sufficiently high and the noise level sufficiently low. Taking more terms

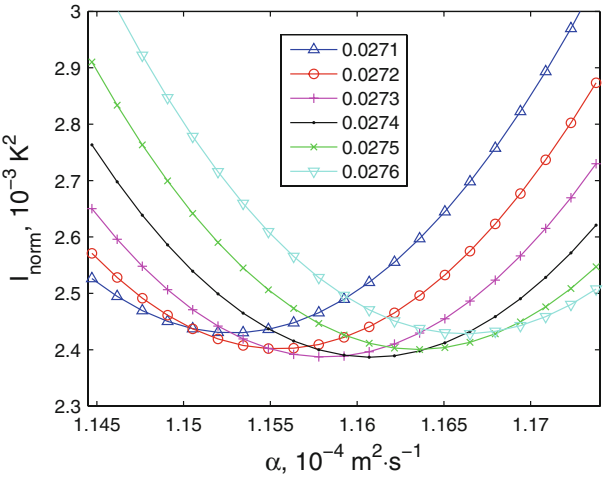

Fig. 7 The value of the cost function (Eq. 5) for a copper sample, divided by the integration area, for several values of α and for different ratios η/α (shown in the inset). The minimum of the cost function corresponds to the best theoretical solution for the experimental data. The minimum was now reached for $\eta/\alpha = 0.0274\,\mathrm{m}^{-1}$ and $\alpha = 1.161 \times 10^{-4}\,\mathrm{m}^2 \cdot \mathrm{s}^{-1}$

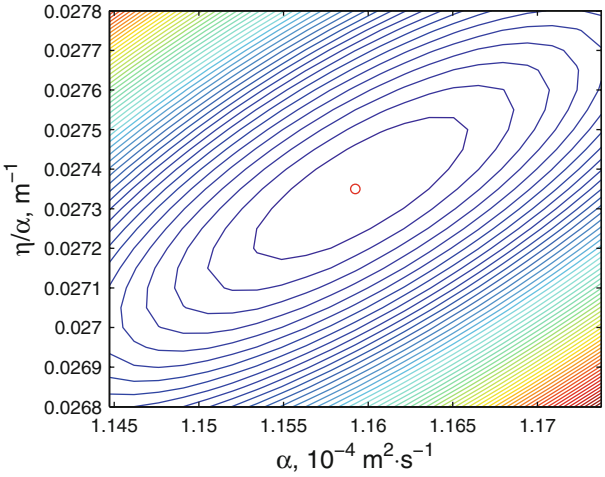

Fig. 8 Normalized cost-function contours for a copper sample in the $(\alpha, \eta/\alpha)$ space. The small circle represents the location of the minimum. The values of the cost function on adjacent contour lines differ by 1 %

in the sum would make Fig. 9 smoother as the ridges would gradually die out, but this would not increase the accuracy by which the thermal diffusion coefficient is determined. To find out if there is a bias in the measured temperature profiles, we plot in Fig. 10 these profiles for a copper sample at one-second time intervals. It is evident from this figure that, if there is a bias, it is in any case smaller than the accuracy of the temperature readings (0.1 K). The minor oscillations in the average profile arise from the discreteness of the recorded signal (7 bits).

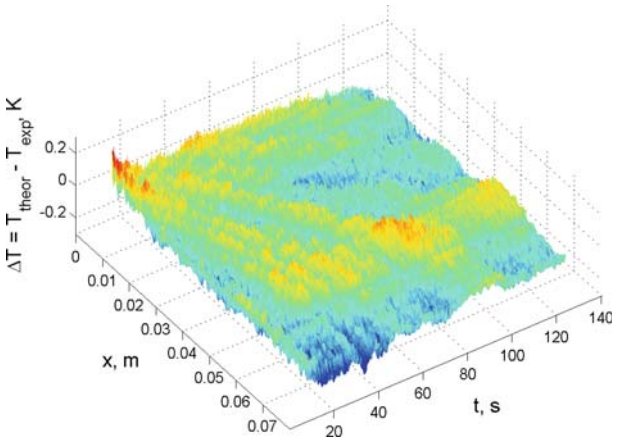

Fig. 9 Difference between the measured temperature data for a copper sample and the theoretical solution of the heat equation calculated by using the best-fit values for the parameters η/α and α

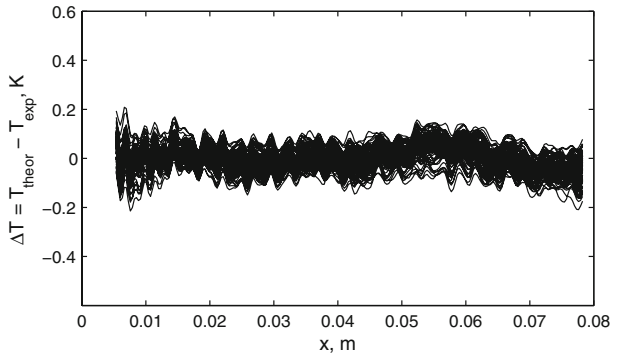

Fig. 10 Cross sections of Fig. 9 at one-second time intervals. The amplitude of temperature variations is similar to (or less than) the accuracy of the measured temperature data, 0.1 K

The procedure described above for determining the thermal diffusion coefficient of a sample was repeated for several independent copper measurements, and also for measurements on an aluminum plate. The results are shown in Table 2. The thermal-conductivity values were determined using the constant density and specific heat values of Table 1. The accuracy of the parameter η/α was $0.0001\,\mathrm{m}^{-1}$, and it was $1.5 \times 10^{-7}\,\mathrm{m}^2 \cdot \mathrm{s}^{-1}$ for parameter α.

The error limits in the individual results of Table 2 are of the order of 0.5 %. This estimate was obtained by changing the integration limits and the moment when the initial temperature profile was taken from measurement data. These changes moved the position of the cost-function minimum by about 0.5 % at the maximum. The mean values of the results shown in Table 2 are (401 and 220) $\mathrm{W} \cdot \mathrm{m}^{-1} \cdot \mathrm{K}^{-1}$ for copper and aluminum, respectively. The corresponding values for the standard deviation of the mean are (3 and 1) $\mathrm{W} \cdot \mathrm{m}^{-1} \cdot \mathrm{K}^{-1}$. Thus, the final results of our measurements are $(401 \pm 3)\ \mathrm{W} \cdot \mathrm{m}^{-1} \cdot \mathrm{K}^{-1}$ and $(220 \pm 1)\ \mathrm{W} \cdot \mathrm{m}^{-1} \cdot \mathrm{K}^{-1}$.

Table 2 Results for individual measurements and averages for copper and aluminum

Sample	η/α (m^{-1})	α ($10^{-3}\,m^2 \cdot s^{-1}$)	k ($W \cdot m^{-1} \cdot K^{-1}$)	I_{norm} (K^2)
Cu	0.0284	0.1169	402.5	0.00304
	0.0306	0.1153	397	0.00415
	0.0294	0.1145	394	0.00314
	0.0274	0.1161	399.5	0.00239
	0.0293	0.1140	392.5	0.00305
	0.0295	0.1148	395	0.00317
	0.0304	0.1193	410.5	0.00311
	0.0311	0.1200	413	0.00288
	0.0308	0.1187	408.5	0.00338
	0.0296	0.1159	399	0.00361
Average		0.1165	401	
Al	0.0488	0.08955	218.5	0.00235
	0.0506	0.08873	216.5	0.00520
	0.0500	0.09037	220.5	0.00350
	0.0478	0.09037	220.5	0.00343
	0.0486	0.09078	221.5	0.00272
	0.0510	0.09140	223	0.00365
	0.0514	0.09058	221	0.00205
	0.0508	0.09037	220.5	0.00239
	0.0509	0.09058	221	0.00186
	0.0519	0.09140	223	0.00249
	0.0505	0.08935	218	0.00291
Average		0.09032	220	

5 Discussion

It was known from independent measurements that for the copper of which our sample was made, the thermal conductivity is $k = 399\,W \cdot m^{-1} \cdot K^{-1}$ with unspecified error bars. This result is based on an electrical-conductivity measurement that is very accurate. Our result agrees well with this value. For high-purity aluminum $k = 237\,W \cdot m^{-1} \cdot K^{-1}$ at 300 K with (2 to 3)% uncertainty [6,1]. Our result falls below the lower limit which can be explained by impurities in the sample that lower the thermal conductivity (see [9]).

The advantages of our method are the one-dimensional form of the heat equation, which is easy to solve and handle experimentally, and that detailed knowledge of the boundary conditions is not required. The contact resistance between the heating elements and the sample has no influence on the final results.

We used here isotropic samples to validate our method, but it is also applicable to determination of the thermal diffusion coefficient for samples that are not isotropic in the x direction (see Fig. 3). The present version of the method requires that the sample is homogeneous in the z direction and that the Biot number related to the sample thickness is small, $Bi_z = ha/k_z \ll 1$. This requirement gives a limit for the sample thickness: $a \ll k_z/h$. For good heat conductors, such as copper and aluminum, $k \sim 100\,W \cdot m^{-1} \cdot K^{-1}$. The convection term in the present setup was $h \sim 10\,W \cdot m^{-2} \cdot K^{-1}$ (see below), so that $k/h \sim 10\,m$. The samples were $10^{-3}\,m$ thick, and the Biot number condition was well satisfied. The method would also work

for poor heat conductors if the sample thickness were sufficiently low. For example, for paper, $k \sim 0.1\,\mathrm{W \cdot m^{-1} \cdot K^{-1}}$ and thus $k/h \sim 10^{-2}\,\mathrm{m}$, and a typical paper thickness is $a \sim 10^{-4}\,\mathrm{m}$. So the Biot number condition would be satisfied also for paper-like materials, but the limiting factor here is that the area of the material where the temperature rises clearly above room temperature would be small, and acquiring enough data might be difficult.

It turned out that shielding of the measuring chamber around the sample is necessary when good-quality temperature data are required. Without shielding reflections of, e.g., hot equipment in the surroundings can be seen in the temperature field of the sample, although it is painted black.

The measuring method is sensitive to convective heat transfer. Uncontrolled air flows around the sample will affect the temperature profiles measured and, consequently, the thermal-conductivity properties determined. We chose to make the convection as constant as possible because in the case of no initial flow at all, free convection would create an unstable heat-transfer field. Since we take the temperature profile as a mean over a narrow strip around the center line of the sample, it is assumed that the convection coefficient h is independent of position. Edge effects in the x direction are also eliminated by reducing the length of the fitting area.

From Table 2 we can also calculate an average value for the parameter η, which consists of both convective and radiative parts as mentioned above. For the copper sample, $\eta\rho c_p = h + 4\varepsilon\sigma T_\infty^3 = (11.9 \pm 0.2)\,\mathrm{W \cdot m^{-2} \cdot K^{-1}}$. The contribution of the radiation is about 50 %, and it cannot be ignored. Furthermore, we can now estimate how accurate is the linearized temperature dependence of the radiation term. For the measurement shown in Figs. 4 and 5, the linearized form $4\varepsilon\sigma T_\infty^3(T - T_\infty)$ gives an about 7 % lower heat flux (on the average) than the fourth-power term $\varepsilon\sigma(T^4 - T_\infty^4)$ of the Stefan–Boltzmann law. This means a 0.5 % error in the flux per 1 K temperature difference between the plate and the surroundings. But for the fit parameter η, the error is only about $0.25\,\% \cdot \mathrm{K^{-1}}$, and this effective temperature dependence is too low to detect when fitting the measurement data.

One can get rid of convective heat transfer by placing the measurement system in vacuum. In this way it would be possible to determine the temperature dependence of the thermal conductivity more accurately (one unknown parameter less), provided that the noise in the temperature data is at a low-enough level. It would also be easier to model heat transfer by radiation through the true Stefan–Boltzmann law.

Acknowledgments We would like to thank Luvata for providing the copper samples. We are grateful to Kimmo Ranttila for making Fig. 1, and to Hannu Rajainmäki for very useful discussions.

Appendix A

Consider the boundary value problem of Eqs. 3 and 4. The substitution of

$$u(x,t) = \Theta(x,t)\mathrm{e}^{\frac{2\eta}{a}t} \tag{A1}$$

leads to the heat equation,

$$\frac{\partial u}{\partial t} = \alpha \frac{\partial^2 u}{\partial x^2} \tag{A2}$$

with the initial and boundary values,

$$\begin{cases} u(x,0) = f(x), \\ u(0,t) = \theta_0(t), \\ \alpha \dfrac{\partial u(L,t)}{\partial x} + \eta u(L,t) = 0, \end{cases} \tag{A3}$$

where $\theta_0(t) = \Theta_0(t) \mathrm{e}^{\frac{2\eta}{a}t}$. The solution of this problem can be written as a sum of the solutions of Eq. A2 with the boundary conditions,

$$\begin{cases} u(x,0) = f(x), \\ u(0,t) = 0, \\ \alpha \dfrac{\partial u(L,t)}{\partial x} + \eta u(L,t) = 0 \end{cases} \tag{A4}$$

and

$$\begin{cases} u(x,0) = 0, \\ u(0,t) = \theta_0(t), \\ \alpha \dfrac{\partial u(L,t)}{\partial x} + \eta u(L,t) = 0. \end{cases} \tag{A5}$$

Consider at first Eq. A2 with the homogeneous boundary conditions, Eq. A4. Separation of variables, $u(x,t) = X(x)T(t)$, leads to the differential equations,

$$\frac{T'(t)}{T(t)} = \alpha \frac{X''(x)}{X(x)} = -\lambda. \tag{A6}$$

For function X we thus find the boundary value problem,

$$\begin{cases} \alpha X'' = -\lambda X \\ X(0) = 0,\ X'(L) + \mu X(L) = 0, \end{cases} \tag{A7}$$

where $\mu = \eta/\alpha$. This eigenvalue problem is easy to solve, and its eigenfunctions are

$$X_n(x) = \sin \beta_n x,\ n = 1, 2, \ldots, \tag{A8}$$

where $0 < \beta_1 < \beta_2 < \ldots$ are the solutions of the equation

$$\mu \tan \beta L = -\beta, \tag{A9}$$

and the corresponding eigenvalues are $\lambda_n = \beta_n^2/\alpha$. By the Sturm–Liouville theorem these eigenfunctions form an orthogonal basis in $L^2([0, L])$. Using standard Fourier-series methods we obtain a solution of the boundary value problem, Eqs. A2 and A4, in the form,

$$u(x,t) = \sum_{n=1}^{\infty} \left(\frac{\mathrm{e}^{-\alpha\beta_n^2 t}}{\gamma_n} \int_0^L f(y) \sin \beta_n y \mathrm{d}y \right) \sin \beta_n x, \tag{A10}$$

where

$$\gamma_n = \int_0^L \sin^2 \beta_n y \mathrm{d}y = \frac{1}{2}\left(L + \frac{\mu}{\beta_n^2 + \mu^2} \right). \tag{A11}$$

By the completeness of the eigenfunctions, we can expand the solution of the inhomogeneous problem, Eqs. A2 and A5, as a Fourier series;

$$u(x,t) = \sum_{n=1}^{\infty} u_n(t) \sin \beta_n x \tag{A12}$$

with the coefficients

$$u_n(t) = \frac{1}{\gamma_n} \int_0^L u(x,t) \sin \beta_n x \mathrm{d}x. \tag{A13}$$

The initial condition $u(x, 0) = 0$ requires that $u_n(0) = 0$. In the same way we can expand the derivatives such that

$$\begin{aligned} \frac{\partial u}{\partial t}(x,t) &= \sum_{n=1}^{\infty} v_n(t) \sin \beta_n x \\ \frac{\partial^2 u}{\partial x^2}(x,t) &= \sum_{n=1}^{\infty} w_n(t) \sin \beta_n x. \end{aligned} \tag{A14}$$

with the coefficients

$$\begin{aligned} v_n(t) &= \frac{1}{\gamma_n} \int_0^L \frac{\partial u}{\partial t}(x,t) \sin \beta_n x \mathrm{d}x \\ w_n(t) &= \frac{1}{\gamma_n} \int_0^L \frac{\partial^2 u}{\partial x^2}(x,t) \sin \beta_n x \mathrm{d}x. \end{aligned} \tag{A15}$$

We easily find that

$$v_n(t) = \frac{\mathrm{d}u_n}{\mathrm{d}t}(t) \quad \text{and} \quad v_n(t) = \alpha w_n(t). \tag{A16}$$

Integrating twice by parts gives

$$w_n(t) = \frac{1}{\gamma_n}\left(\frac{\partial u}{\partial x}(L,t)\sin\beta_n L - \beta_n u(L,t)\cos\beta_n L + \beta_n u(0,t) - \beta_n^2 \int_0^L u(x,t)\sin\beta_n x \mathrm{d}x\right). \tag{A17}$$

Using the boundary conditions of Eqs. A5 and A9, we find that

$$w_n(t) = \frac{\beta_n}{\gamma_n}\theta_0(t) - \beta_n^2 u_n(t). \tag{A18}$$

We finally find the differential equation,

$$\frac{\mathrm{d}u_n}{\mathrm{d}t} = -\alpha\beta_n^2 u_n + \frac{\alpha\beta_n}{\gamma_n}\theta_0(t), \quad u_n(0) = 0, \tag{A19}$$

for the functions u_n. The solution of this equation is

$$u_n(t) = \frac{\alpha\beta_n \mathrm{e}^{-\alpha\beta_n^2 t}}{\gamma_n}\int_0^t \mathrm{e}^{\alpha\beta_n^2 s}\theta_0(s)\mathrm{d}s. \tag{A20}$$

The solution of our original boundary value problem, Eqs. 3 and 4, can thus be expressed in the form

$$\Theta(x,t) = \sum_{n=1}^{\infty}\frac{\mathrm{e}^{-(\alpha\beta_n^2+2\eta/a)t}}{\gamma_n}\left(\int_0^L f(y)\sin\beta_n y\mathrm{d}y + \alpha\beta_n \times \int_0^t \mathrm{e}^{(\alpha\beta_n^2+2\eta/a)s}\Theta_0(s)\mathrm{d}s\right)\sin\beta_n x. \tag{A21}$$

Note that this solution is not continuous at the boundary $x = 0$. The boundary conditions are satisfied in the limit $\lim_{x\to 0+}\Theta(x,t) = \Theta_0(t)$. We have to take the Gibbs' phenomenon into account while using this solution in the numerical computations. It means that in the optimization problem Eq. 5, we must take $x_1 > 0$.

References

1. Y.S. Touloukian, C.Y. Ho, *Thermophysical Properties of Matter: Thermal Conductivity of Metallic Solids* (Plenum Press, New York, 1972)
2. W.J. Parker, R.J. Jenkins, C.P. Butler, G.L. Abbott, J. Appl. Phys. **32**, 1679 (1961)
3. For a recent review, see, e.g., L. Vozár, W. Hohenauer, High Temp-High Press. **35/36**, 253 (2003/2004)
4. I. Philippi, J.C. Batsale, D. Maillet, A. Degiovanni, Rev. Sci. Instrum. **66**, 182 (1995)
5. B. Rémy, A. Degiovanni, D. Maillet, Int. J. Thermophys. **26**, 493 (2005)
6. F.P. Incropera, D.P. DeWitt, *Fundamentals of Heat and Mass Transfer*, 5th edn. (Wiley, New York, 2002), pp. 905–908
7. N.J. Simon, E.S. Drexler, R.P. Reed, Properties of copper and copper alloys at cryogenic temperatures. *NIST Monograph 177* (1992)
8. J.G. Hust, A.B Lankford, Thermal conductivity of aluminum, copper, iron, and tungsten for temperatures from 1 K to the melting point. *NBSIR 84-3007* (1984)
9. R. Berman, *Thermal Conduction in Solids* (Clarendon Press, Oxford, 1976), pp. 143–168